*Clays and Clay Minerals*, Vol. 48, No. 3, 339–350, 2000.

# ELECTRON MICROSCOPY STUDY OF VOLCANIC TUFF ALTERATION TO ILLITE-SMECTITE UNDER HYDROTHERMAL CONDITIONS

S. DE LA FUENTE,[1] J. CUADROS,[1] S. FIORE,[2] AND J. LINARES[1]

[1]Estación Experimental del Zaidín, CSIC, Profesor Albareda, 1, 18008 Granada, Spain
[2]Istituto di Ricerca sulle Argille, CNR, Via S. Loja, 85050 Tito Scalo (Pz), Italy

**Abstract**—Experimental alteration of volcanic tuff from Almería, southeastern Spain, was performed in solutions with different Na/K ratios (0.01, 1, 10, and 100), different total salt concentrations (0.01, 0.1, 0.2, 0.33, and 1 M), and in deionized water, at 60, 80, 120, and 160°C, for periods of 60, 90, 180, and 360 d. Two particle size fractions of volcanic tuff were used: 10–200 and 20–60 μm. Alteration products were examined by X-ray diffraction (XRD), Fourier-transform infrared spectroscopy (FTIR), laser-particle size analysis, scanning electron microscopy equipped with an energy dispersive X-ray spectrometer (SEM-EDS), image computer analysis, and transmission electron microscopy with microanalysis (TEM-AEM). XRD detected neoformed phases only in the products from experiments of 180–360 d at high temperatures (120–160°C), and with Na/K ratios above unity and in deionized water. The synthesized phase is a random mixed-layer illite-smectite (I-S) with 75% smectite. The quantity of newly formed I-S, determined by FTIR, ranged between 3–30%. There was no apparent change in grain size and shape of the grains after the experiments as compared to before.

SEM-EDS and TEM-AEM revealed the following alteration sequence: 1) intense etching on glass-grain surfaces; 2) formation of hemispherical morphologies on grain surfaces; 3) precipitation of very thin, individual flakes of illite-smectite on glass-grain surfaces; 4) development of I-S at the edges of glass grains; and 5) development of I-S honeycomb structures either covering large areas of the glass grains or resulting from the complete alteration of glass grains. A direct transformation of glass to I-S seems to be the major reaction mechanism, although there also is evidence of glass dissolution and subsequent I-S precipitation.

**Key Words**—Hydrothermal Alteration, Illite-Smectite, SEM-EDS, TEM-AEM, Volcanic Tuff.

## INTRODUCTION

Volcanic glass is not stable under ambient conditions and transforms to various thermodynamically more stable secondary phases depending on glass composition, texture, and other physical and chemical conditions. Most studies on natural glass alteration focus mainly on the secondary phases and not on the specific conditions of time, temperature, and fluid composition of the alteration process. For conditions of short times of alteration and/or low temperatures, glass-like or poorly crystalline phases are common (Crovisier *et al.*, 1982; Magonthier *et al.*, 1992; Kawano *et al.*, 1997). Higher temperatures and longer periods promote greater crystallinity and phases such as smectite and zeolite. Hofmann and Jager (1959) found that glass of basaltic composition favors the formation of saponite, whereas Banfield and Barker (1998) reported the formation of zeolite from alkali-bearing tuff. Caballero (1985) found that hydrothermal solutions of granitic composition favored smectite formation, and McDaniel *et al.* (1995) reported beidellite from tephra in the presence of water with low pH and with organic metal-complexing agents. Berkgaut *et al.* (1994) found illite-smectite (I-S) in soils developed on pyroclastics where there was an alternation of humid and dry seasons. Halloysite and kaolinite dominate in a humid climate in soils formed form volcanic ash and pumice (Wada, 1987). Banfield and Barker (1998) found smectite formation is favored by low porosity and where ion concentrations are high.

Experimental alteration of volcanic glass allows better control and understanding of these conditions and the effect on the secondary phases. Kinetic effects (*e.g.*, low temperatures, short alteration times) influence the formation of poorly crystalline phases such as hydrotalcite (Abdelouas *et al.*, 1994) and allophane (Kawano and Tomita, 1992, 1995; Kawano *et al.*, 1993). Low pH promotes the formation of halloysite and kaolinite (Nagasawa, 1978; Kawano and Tomita, 1995), neutral and slightly basic conditions favor smectite formation (Kawano *et al.*, 1993; Ghiara *et al.*, 1993; Kawano and Tomita, 1997), and basic pH values promote zeolite formation (Mariner and Surdam, 1970; Kawano and Tomita, 1997; Hall, 1998). Na availability may be a factor, with higher Na concentrations in solution favoring smectite over zeolite (Keene *et al.*, 1976; Tomita *et al.*, 1993).

Illite and I-S are also found as products of glass transformation. They are frequently interpreted as a result of illitization of previously formed smectite (Amouric and Olives, 1991; Inoue *et al.*, 1990, 1992; Šucha *et al.*, 1993; Drits *et al.*, 1996). Nevertheless, hydrothermal alteration of volcanic rocks to illite may not be the product of progressive illitization of smectite. Hydrothermal alteration may involve illite or I-S formation directly from a glass precursor (Lanson and Champion, 1991; Zevenbergen *et al.*, 1996).

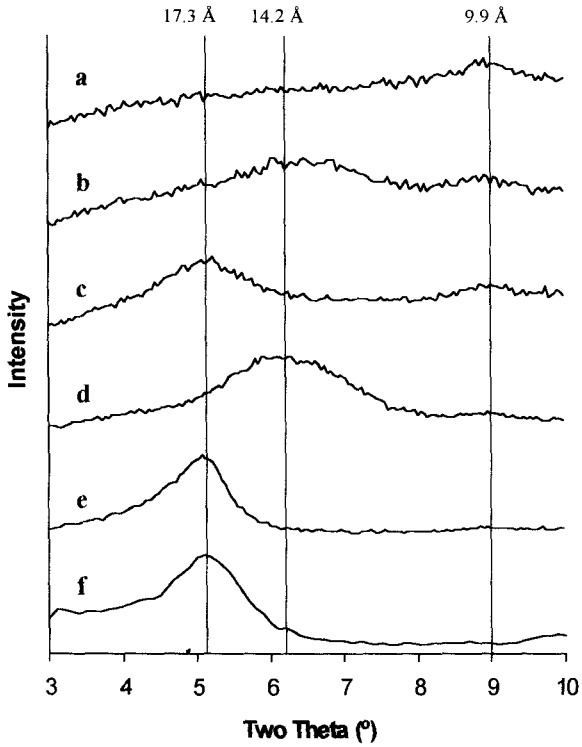


Figure 1. X-ray diffraction patterns of oriented-aggregate mounts of some reaction products. All samples are <2-μm size fraction and Ca exchanged. (a) 80°C, 60 d, Na/K = 10, 0.33 M total salt concentration. (b) 160°C, 180 d, deionized water, air-dried. (c) 160°C, 180 d, deionized water, glycolated. (d) 160°C, 360 d, deionized water, air-dried. (e) 160°C, 360 d, deionized water, glycolated. (f) NEWMOD-simulated pattern of (e).

Reported mechanisms of volcanic glass alteration include the following: 1) formation of an alteration layer on the glass surface by incongruent glass dissolution and selective trapping of dissolved ions (Thomassin *et al.,* 1989; Magonthier *et al.,* 1992; Kawano *et al.,* 1993), 2) congruent dissolution of glass and precipitation of new phases (Crovisier *et al.,* 1992), and 3) formation of protocrystalline domains within the glass that evolve to new crystalline phases (Tazaki *et al.,* 1989; Fiore *et al.,* 1999). The latter mechanism implies long ion-diffusion paths through the glass.

Our experiments address the early stages of volcanic tuff alteration. The experiments, performed at various temperatures, Na and K concentrations, and durations, produced smectite-rich I-S. We observed a direct transformation of the glass to I-S at the surface of the glass particles, along with glass dissolution and I-S precipitation.

## MATERIALS AND METHODS

The volcanic glass used in this study was collected from the volcanic region of Cabo de Gata, Almería, southeastern Spain. The deposit is comprised of pyroclastic materials, ejected in eruptive episodes during the upper Tortonian (Miocene) (Bellon, 1976; Bellon *et al.,* 1983; Di Battistini *et al.,* 1987; Fernández Soler, 1992). The tuff is rhyolitic and is locally and partially altered to bentonite in association with extensive fracturing (Linares, 1985).

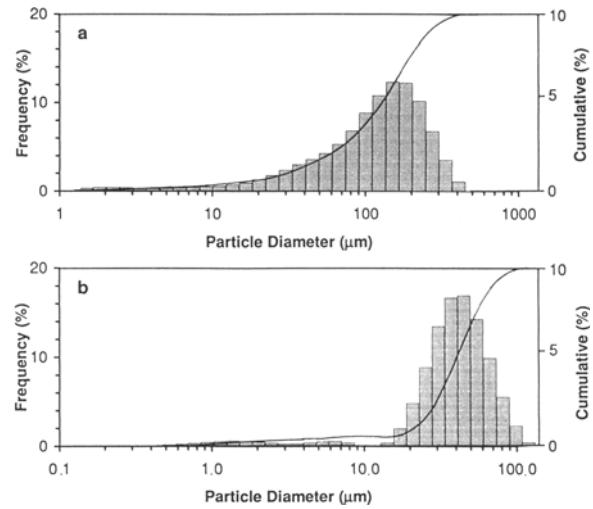


Figure 2. Particle-size distribution of the starting material determined by laser analysis. (a) Particle size of 10–200 μm. (b) Particle size of 20–60 μm.

The tuff was crushed and homogenized in an agate mortar. Powder X-ray diffraction (XRD) (Philips PW 1710 diffractometer with CuKα radiation, automatic divergence slit, and graphite monochromator) showed smectite and trace amounts of biotite, amphibole, quartz, potassium feldspar, plagioclase, and pyroxenes. Smectite concentration in the tuff was determined by thermogravimetry (TG) (Netzsch simultaneous thermal apparatus STA 409 EP) using an approximate sample weight of 50 mg, $Al_2O_3$ as a reference, a temperature range of 20–1020°C, and a heating rate of 10°C/min. We assumed that weight loss at ~620°C corresponded to smectite dehydroxylation (Mackenzie, 1970) and an ideal weight loss of 5% for smectite dehydroxylation (Brindley and Lemaitre, 1987). TG indicated smectite in the amount of 16 wt. %. The amount of smectite might be overestimated owing to water loss from the glass at ~620°C. The tuff was then heated at 900°C for 2 h to destroy the smectite. This product was used as "starting material".

The chemical composition of the starting material was determined by wet chemical analysis. Silicon, Al, and Fe were analyzed by spectrophotometry, using the methods of molibdate blue, alizarin red-S, and ortofenantrolin complexes, respectively (Shapiro, 1975). Calcium and Mg were determined by atomic absorption, and Na and K by flame emission spectroscopy. Two sets of samples were sedimented by settling, one

https://doi.org/10.1346/CCMN.2000.0480305 Published online by Cambridge University Press

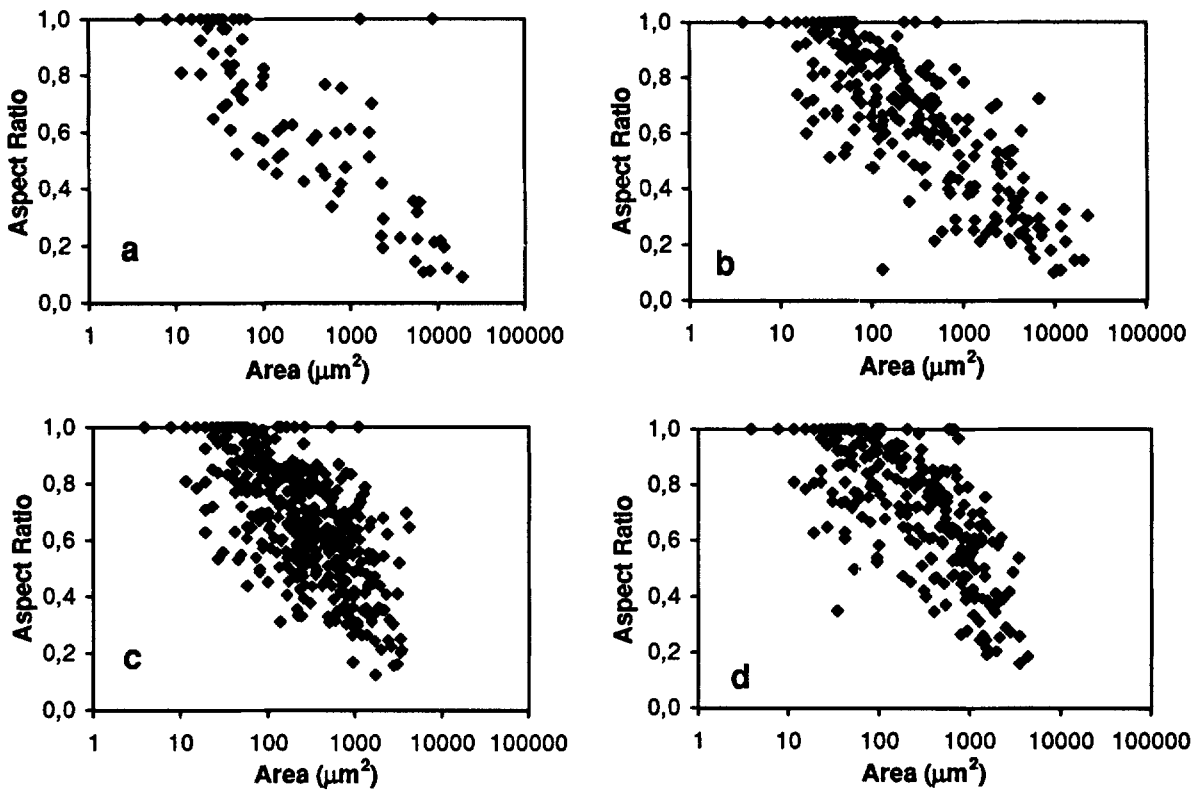


Figure 3. Aspect ratio *vs.* the areas of the particles in the two starting materials and two of their reaction products. (a) Starting material with a particle-size range of 10–200 μm. (b) From starting material of 10–200 μm; reaction conditions 80°C, 360 d, Na/K in solution 0.1, total cation concentration 0.33 M. (c) Starting material of 20–60 μm. (d) From starting material of 20–60 μm; reaction conditions 160°C, 60 d, Na/K in solution 0.01, total cation concentration 0.01 M.

with a grain size of 10–200 μm, and the other with a range of 20–60 μm. The two particle-size groups allow the determination of the influence of grain size on alteration. Samples were placed in steel reactors with a Teflon liner and various salt solutions (5 g/25 mL). The solutions contained NaCl and KCl with Na/K ratios of 0.01, 1, 10, and 100, and with a total salt concentration of 0.01, 0.1, 0.2, 0.33, and 1 M for each Na/K ratio. Other experiments used deionized water. The durations of the experiments were 60, 90, 180, and 360 d at 60, 80, 120, and 160°C. The total pressure inside the reactor vessels was that of equilibrium for water vapor at the corresponding temperature. After each experiment, solutions and solids were separated by centrifugation and analyzed. The <2-μm size fraction was extracted by centrifugation, Ca exchanged with 1 M $CaCl_2$, and washed with deionized water until no $Cl^-$ was detected with $AgNO_3$. The <2-μm products were analyzed by XRD as oriented-aggregate mounts, both air-dried and glycolated. A slow scan speed (0.0034 °2θ/step, 15-s count time) was utilized to improve the signal-to-noise ratio. The XRD patterns were compared against calculated patterns using the NEWMOD program (R.C. Reynolds, Hanover, New Hampshire, USA). The glass/clay ratios in the alteration products were determined by Fourier-transform infrared (FTIR) (Nicolet 20SXB, 500 spectra collected for each analysis, 2 $cm^{-1}$ of resolution), using integrated intensities of the OH stretching band of smectite, I-S, and illite, at ~3620 $cm^{-1}$ (Farmer, 1974). Mixtures of volcanic glass and smectite in known proportions were used to calibrate the integrated intensities of the bands.

Scanning electron microscopy (SEM) (Cambridge Stereoscan S360) coupled with energy dispersive X-ray spectrometry (EDS) (LINK ISIS300) of the starting material and reaction products was performed using a voltage of 20 kV and a working distance of 7 mm for SEM observation and 26 mm for EDS analysis. Transmission electron microscopy (TEM) with microanalysis (AEM) was also performed (Philips CM-20 equipped with a Kevex Quantum solid-state EDX detector) for the starting material and the <2-μm size fraction of the products. AEM analyses were performed in scanning transmission (STEM) mode at 200 kV, using a spot diameter of 70 Å. Collection time was 30 s for Na and K, and 200 s for other elements. X-ray emission coefficients for the different elements

https://doi.org/10.1346/CCMN.2000.0480305 Published online by Cambridge University Press

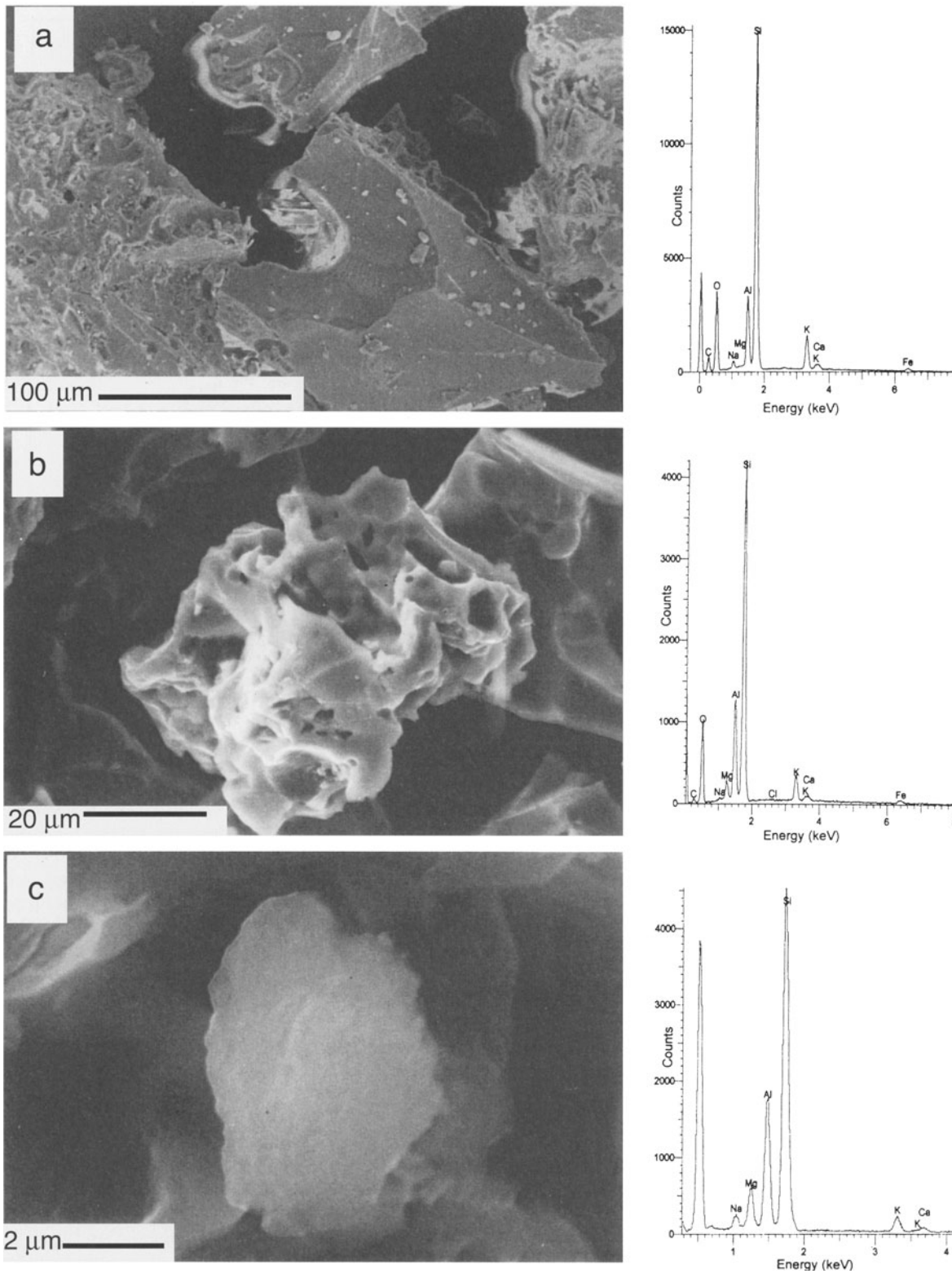


Figure 4. SEM micrographs and EDS spectra of the starting material. EDS peak at 0 keV is an artifact from the detector. (a) Glass grains with a clean surface. (b) Pumice grain. (c) Particle similar to smectite in morphology and chemical composition. This particle is probably smectite dehydroxylate. Unlabeled peak at 0.5 keV corresponds to oxygen.

https://doi.org/10.1346/CCMN.2000.0480305 Published online by Cambridge University Press

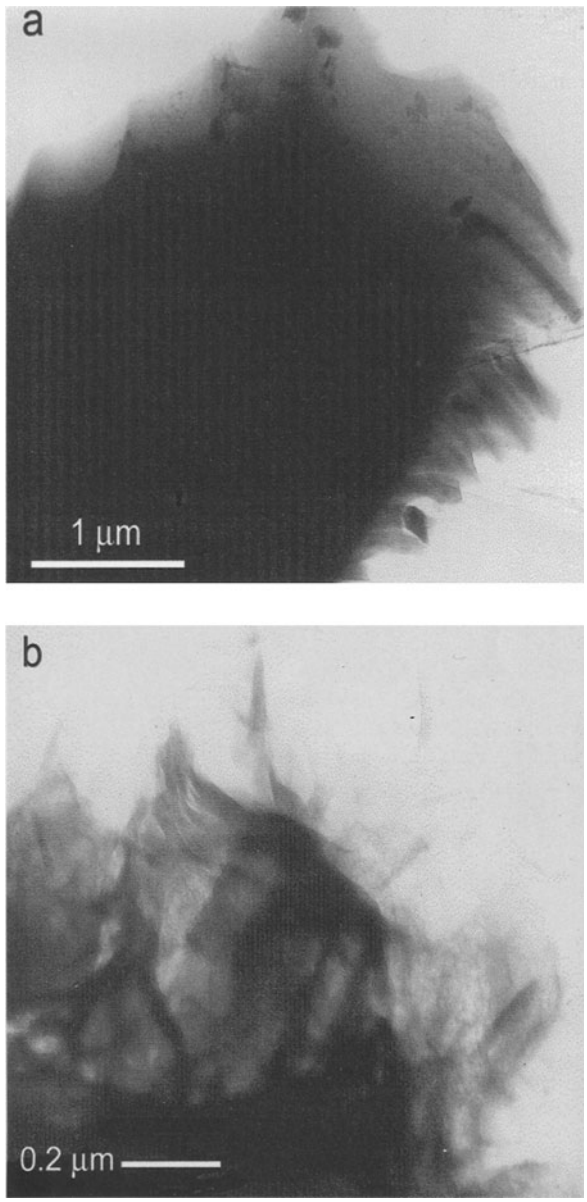


Figure 5. TEM micrographs of the starting material. (a) Fresh glass grain. Si/Al atom ratio is 4.8. (b) Particle with a morphology similar to that of smectite. The Si/Al ratio is 3.2, approaching that of smectite. This particle is probably dehydroxylated smectite.

were determined by analysis of standards. For SEM, we placed a drop of a dispersion of the sample on a carbon stub. The samples were then carbon coated. For TEM, a drop of the material dispersed in ultrapure ethyl alcohol was placed on a Cu microgrid covered with a Formvar film stabilized with carbon. Analyses of I-S in the products were used to calculate structural formulae based on 22 negative charges [$O_{10}(OH)_2$]. All Si and necessary Al summing to four atoms were assigned to the tetrahedral sites. All Fe, remaining Al, and Mg summing to two atoms were assigned to the octahedral sites. Sodium, K, Ca, and remaining Mg were assigned to interlayer sites.

The size distribution of the particles in the starting material and products was analyzed with a laser particle-size analyzer (Malvern MasterSizer/E). The dispersion was constantly stirred during measurements to avoid particle sedimentation. A quantitative study of morphology of the starting material and products was made by SEM and image analysis. Samples were embedded in resin and thin sections prepared. SEM photographs were taken of mounts containing from 149 to 912 particles. Grains presented a clear contrast against the resin background. Photographs were digitized with an image scanner and analyzed using an image analysis program (Mip4adv) to determine particle areas and aspect ratio. The aspect ratio was calculated from $4\ \pi$ area/(perimeter)$^2$. The aspect ratio of a circle is one, and any other geometry has an aspect ratio between zero and one, with higher values as the particle becomes more similar to a circle.

*Description of the starting material*

The chemical composition of the starting material was: 72.89 wt. % $SiO_2$, 14.47 wt. % $Al_2O_3$, 1.25 wt. % $Fe_2O_3$, 1.44 wt. % MgO, 0.86 wt. % CaO, 3.34 wt. % $Na_2O$, and 4.97 $K_2O$.

XRD analysis (Figure 1) at low scan speed of oriented mounts of the material with particle size range of 10–200 μm revealed a broad peak of low intensity at ~10 Å, similar to that in Figure 1a, and this peak was not affected by glycolation. This peak is probably related to smectite that did not completely decompose by calcination. Analysis of the material with the size range of 20–60 μm did not show any crystalline phase. Presumably, the smectite contaminants are present in the smaller glass shards and are less abundant in the size range of 20–60 μm.

Particle size distributions of the starting material for the 10–200 and 20–60-μm size ranges are shown in Figure 2. The size distributions based on the laser technique are in good agreement with the sedimentation process used to separate the size fractions; 90% of the particles are in the corresponding range. For the 10–200-μm size range (Figure 2a), the distribution has a maximum at ~150 μm and a tail towards lower sizes. For the 20–60-μm size range (Figure 2b), the distribution has a tail on the low-size side and a maximum at ~40 μm.

The shape analysis is illustrated by Figure 3, where the aspect ratio *versus* the area of the particles is plotted. Figure 3a and 3c corresponds to the starting material with size ranges of 10–200 and 20–60 μm, respectively. For both size ranges, smaller particles are more rounded in shape. Data points in Figure 3c have a lower maximum area than those in Figure 3a, in agreement with the different size ranges.

https://doi.org/10.1346/CCMN.2000.0480305 Published online by Cambridge University Press

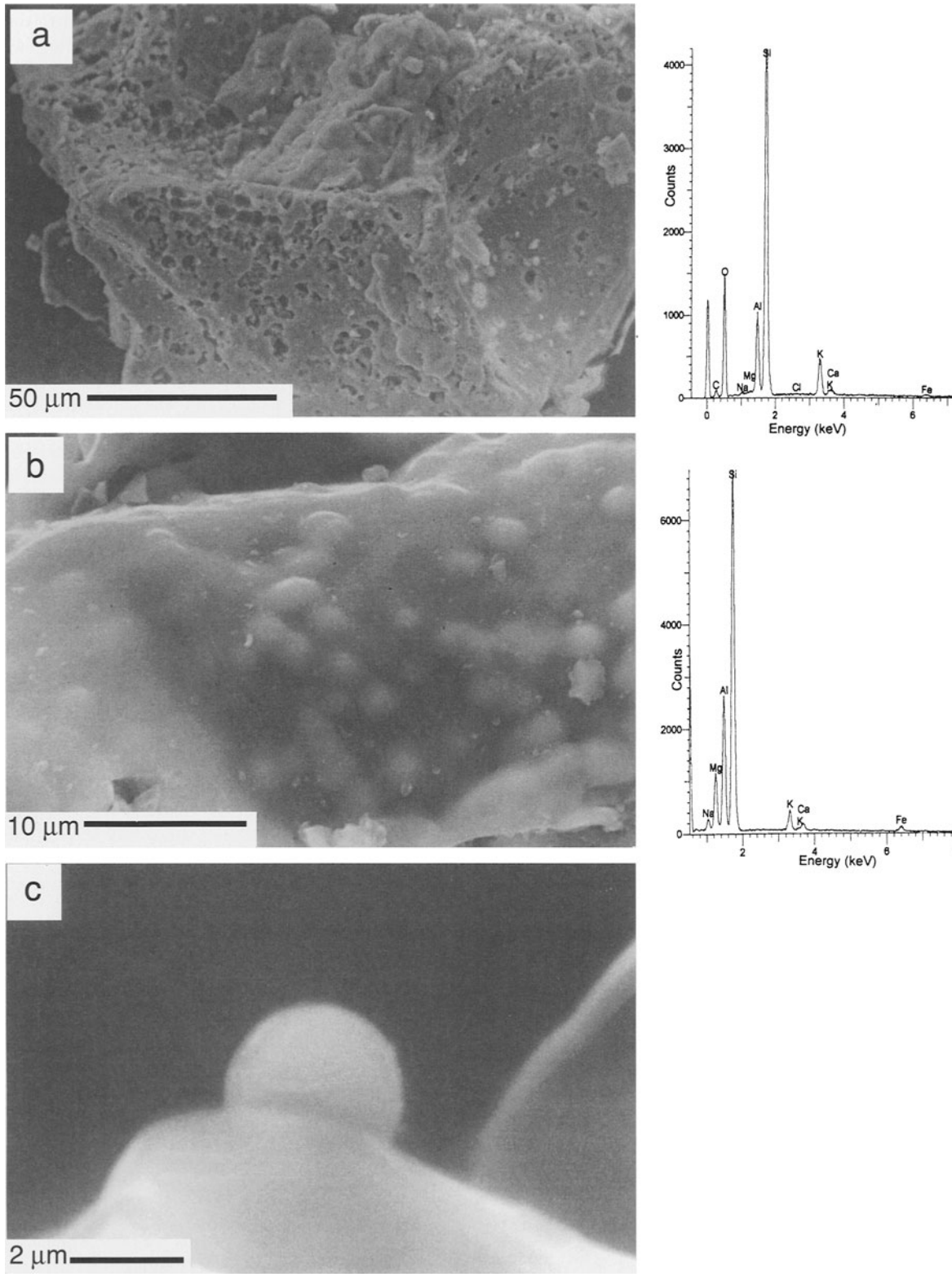


Figure 6. SEM micrographs and EDS spectra of reaction products. EDS peak at 0 keV is an artifact from the detector. (a) Glass grain with etch pits produced by dissolution. (b) Hemispherical structures on a grain surface. (c) Detail of a hemispherical structure on the surface of a glass grain. (d) Very thin flakes on the surface of a glass particle. (e) Smectite-like flakes forming ball-shaped structures found on the inner surface of holes in some altered grains. (f) Honeycomb structures. The grains are extensively altered but preserve their external shape.

https://doi.org/10.1346/CCMN.2000.0480305 Published online by Cambridge University Press

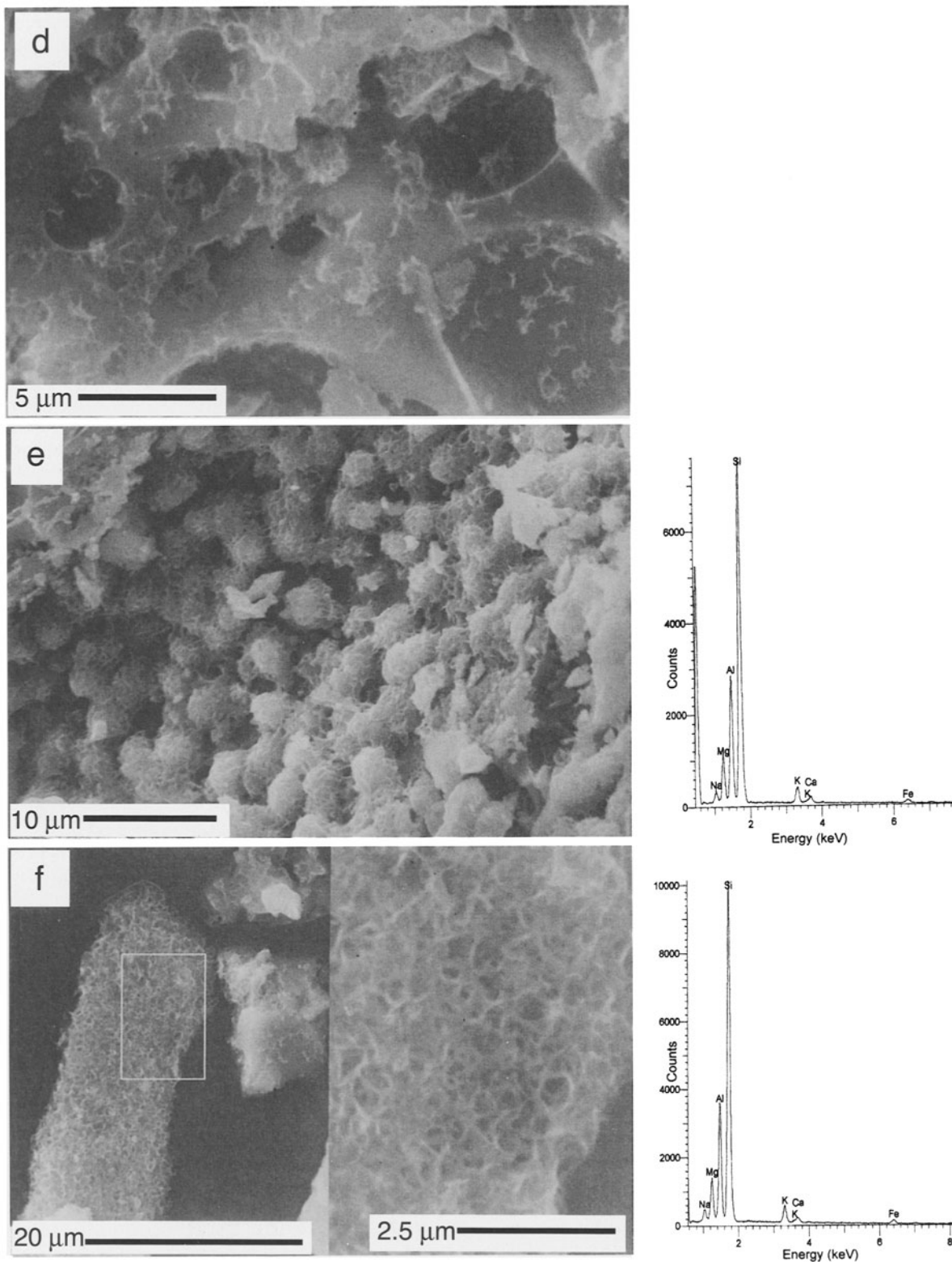


Figure 6. (Continued)

https://doi.org/10.1346/CCMN.2000.0480305 Published online by Cambridge University Press

SEM-EDS study of the starting material (10–200 and 20–60 μm) showed that it consists of equidimensional glass grains with shard morphology, particles similar to smectite in morphology, and a few particles of potassium feldspar and pyroxene. The smectite-like grains are more abundant in the material with grain size of 10–200 μm. Glass particles are differentiated into two populations by morphology. The more abundant population is comprised of particles with clean surfaces (Figure 4a). The other particles have altered-appearing surfaces, containing vesicles (Figure 4b). The chemical compositions of both sets are similar, with Si and Al as the abundant elements, and K, Na, Ca, and Fe in lesser amounts. Mg is also present in some vesiculated grains. Platy flakes, similar to smectite in morphology and composition (Figure 4c), cluster to form massive aggregates. We assume these aggregates are dehydroxylated smectite that did not decompose during calcination.

TEM-AEM analysis showed that the starting material consists mainly of glass grains that are easily distinguished because of sharp edges and dark contrast owing to thickness (Figure 5a). They have a rhyolitic composition, with Si/Al atomic ratios typically ranging from 3 to 5, with a mean value of 4. Less-abundant particles occur with morphologies and chemical compositions consistent with or approaching those of smectite (Figure 5b). These are probably dehydroxylated smectite particles from calcination as observed by XRD and SEM. These particles do not show electron diffraction patterns, probably owing to low crystallinity.

## RESULTS

### *XRD*

XRD patterns of the reaction products with an original particle-size range of 10–200 μm varied depending on reaction duration, temperature, and solution composition. Products of the experiments at 60–90 d have only a very broad and weak reflection at ~10 Å, which is not affected by glycolation (Figure 1a). This peak was also present in the starting material of the corresponding size range. XRD patterns of products from experiments of 180–360 d, temperatures of 120–160°C, and Na/K ratios above one or in deionized water have a peak at 14 Å that occurs at 17 Å upon glycolation, and the 10-Å peak becomes weaker or is absent (Figure 1b and 1c). The peak at 14 and 17 Å becomes sharper and more intense with increasing time (360 d), temperature (160°C), and with deionized water, but the absolute intensity is always low and no additional peaks develop (Figure 1d and 1e). The peak at 14 and 17 Å is compatible with smectite or smectite-rich I-S. The products contain glass and 3–30 wt. % of smectite or smectite-rich I-S, as determined by FTIR. Smectite or I-S patterns calculated by NEWMOD were mixed with the experimental XRD patterns of a glass in the glass/clay proportions initially obtained by FTIR. The mixing function is also performed by NEWMOD. The resulting best fit was for a random interstretified I-S with 75% smectite based on the glycolated samples (Figure 1e and 1f). The air-dried specimens could not be correctly simulated, possibly because of the presence of expandable layers with variable water contents. XRD patterns for the experiment with particle sizes of 20–60 μm did not show crystalline phases.

### *Particle-size and particle-morphology analyses*

The particle-size distributions for the reaction products (not shown) are similar to Figure 2 with minor variations. Multiple analyses of a same sample to show the precision of the analysis indicated apparent differences that were statistically significant. Thus, these data are of limited value, but the results do suggest that the differences of the particle-size distribution between the starting material and products are not large, because they are of the same magnitude or smaller than those found between analyses of the same sample.

The image analysis of the SEM micrographs of the products did not show any morphology change with respect to the starting material for any of the experiments. Figure 3b and 3d shows the result of the morphology data for two products of the experiments involving the size fractions of 10–200 and 20–60 μm, respectively. The distribution of data points is similar to that of the corresponding starting material (Figure 3a and 3c).

### *Electron microscopy*

SEM-EDS examination of the reaction products (10–200 and 20–60 μm) showed four features that developed over time and reaction temperature, without apparent influence of the solution composition, in the following sequence: (1) Glass grains with an etched surface are apparently related to non-homogeneous glass dissolution (Figure 6a). This etching is not observed in the starting material and, hence, it occurred during the experiments. Etched grains are common for all reaction products, and the composition is similar to unaltered grains (compare EDS spectra in Figures 4a and 6a). (2) Hemispherical structures on the surface of the glass grains are probably the result of incomplete glass alteration (Figure 6b and 6c). This morphology was described previously as a result of hydrothermal alteration of natural and synthetic glass (Tazaki *et al.*, 1989, 1992; Fiore, 1993). The chemical composition of the glass surfaces at this feature is similar to smectite. (3) Very thin flakes on grain surfaces (Figure 6d) are abundant in all samples, even at the early stages of alteration. The small size precluded chemical analysis. (4) Honeycomb structures with a chemical com-

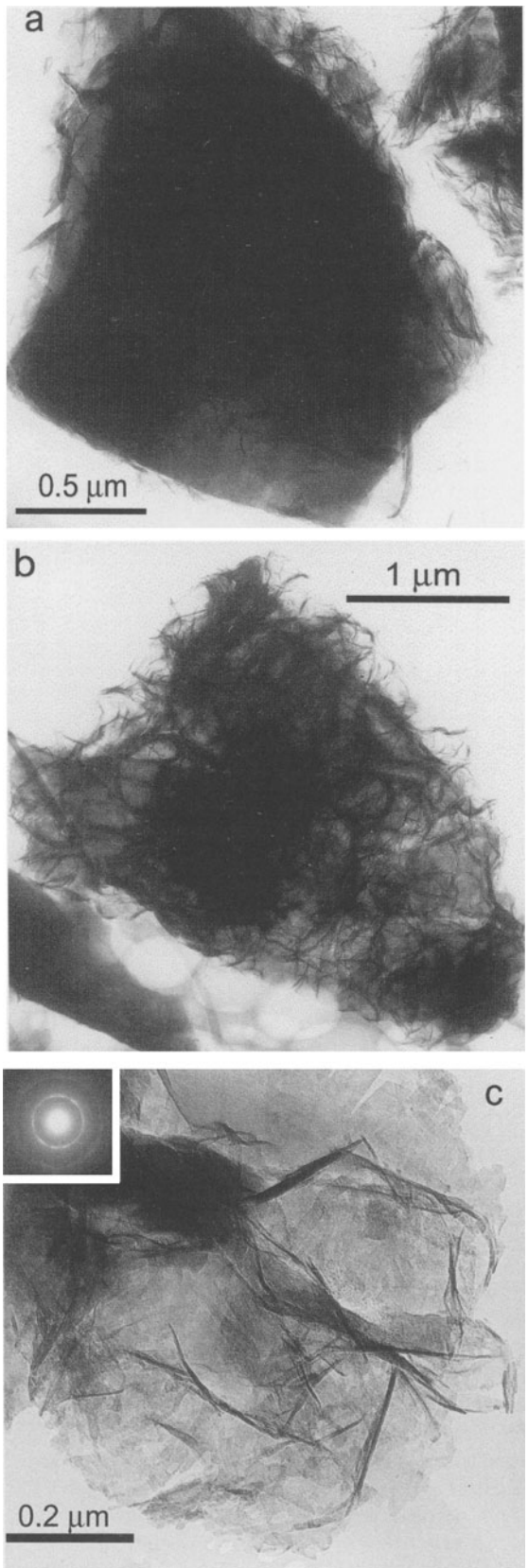


position consistent with smectite are present in two different arrangements. Some occur in ball-shaped units (Figure 6e) and cover the inner surface of holes in some grains. They were observed in the most altered samples (360 d, 160°C, and in deionized water). In the other arrangement, the flakes uniformly cover the grain surface, and the external morphology of the original grain is preserved even where the grain appears to be greatly altered (Figure 6f).

The <2-μm size fraction was used in the TEM-AEM study to concentrate the reaction products. The morphologies for the two sets of particle size are similar and are described together. Grains analyzed by AEM show a wide range of Si composition. Those with little or no signs of alteration have higher Si contents. Many particles with a smectite-like morphology have a composition similar to smectite, some of them with excess Si. Calculated structural formulae of the materials without such Si excess are given in Table 1. Octahedral occupancies are between 1.91–2.08. The layer charge is in the range of smectite-rich I-S in most cases, in agreement with the XRD results, although some of the layer-charge values are typical for illite-rich I-S and illite.

The observed alteration sequence over time and temperature is the following: (1) Fresh grains, generally of large size are similar to those in the starting material. They are more abundant in samples from experiments of short duration and/or low reaction temperatures. (2) Glass grains occur with edges altered to smectite-like flakes (Figure 7a). These grains are frequently of small size (1–2 μm). Edge alteration is also apparent by chemical analysis, so that the composition varies from the core to the edge. Rims showing the most advanced alteration are products from experiments of long duration, but altered rims are present in products of 60 d of alteration. Altered rims have a chemical composition similar to smectite-rich I-S and some (from experiments of 90–360 d) show electron diffraction patterns consisting of rings indicative of turbostratic stacking. (3) Particles occur with a glass-grain outline but with an interior texture and contrast, indicating an advanced state of alteration (Figure 7b). These grains are altered to smectite-rich I-S, as indicated by chemical analysis, but they commonly maintain the original external shape. These particles do not

←

Figure 7. TEM micrographs of the reaction products. (a) Glass grain with edges altered to smectite-like flakes. Si/Al atom ratio is 3.4 in the core, and 3 in the altered rim. (b) Particle with a glass-grain outline completely altered to smectite-rich I-S. AEM analysis yields the structural formula number 18 in Table 1. Si/Al ratio is 2.7. (c) Particle of smectite-rich I-S and its electron diffraction pattern. AEM analysis yields the structural formula number 1 in Table 1. Si/Al ratio is 2.4.

https://doi.org/10.1346/CCMN.2000.0480305 Published online by Cambridge University Press

Table 1. Structural formulae of I-S particles obtained by AEM. They are listed in order of increasing layer charge.

| | T (°C) | Time (d) | Na/K | Tot. conc. (M) | Si | $^{IV}$Al | $^{VI}$Al | $^{VI}$Mg | $^{VI}$Fe | Na | K | Ca | Mg | Σ oct. | Layer charge |
|---|---|---|---|---|---|---|---|---|---|---|---|---|---|---|---|
| 1 | 160 | 180 | 0.01 | 1.00 | 3.94 | 0.06 | 1.56 | 0.31 | 0.13 | 0.00 | 0.05 | 0.09 | 0.07 | 2.00 | 0.37 |
| 2 | 160 | 90 | d.w. | 0 | 4.09 | 0.00 | 1.44 | 0.50 | 0.06 | 0.00 | 0.05 | 0.15 | 0.03 | 2.00 | 0.41 |
| 3 | 160 | 180 | 100 | 1.00 | 3.98 | 0.02 | 1.45 | 0.40 | 0.15 | 0.00 | 0.07 | 0.09 | 0.08 | 2.00 | 0.41 |
| 4 | 80 | 60 | 0.01 | 1.00 | 3.34 | 0.66 | 1.98 | 0.00 | 0.10 | 0.00 | 0.20 | 0.04 | 0.07 | 2.08 | 0.42 |
| 5 | 160 | 180 | 100 | 1.00 | 3.94 | 0.06 | 1.48 | 0.39 | 0.14 | 0.00 | 0.10 | 0.06 | 0.12 | 2.00 | 0.45 |
| 6 | 80 | 90 | 0.01 | 1.00 | 3.86 | 0.14 | 1.59 | 0.32 | 0.09 | 0.00 | 0.02 | 0.07 | 0.16 | 2.00 | 0.46 |
| 7 | 160 | 90 | d.w. | 0 | 4.01 | 0.00 | 1.48 | 0.47 | 0.05 | 0.00 | 0.05 | 0.14 | 0.06 | 2.00 | 0.46 |
| 8 | 80 | 60 | 0.01 | 1.00 | 3.48 | 0.52 | 1.87 | 0.00 | 0.15 | 0.00 | 0.10 | 0.06 | 0.13 | 2.02 | 0.47 |
| 9 | 160 | 180 | 100 | 1.00 | 3.81 | 0.19 | 1.58 | 0.30 | 0.12 | 0.00 | 0.04 | 0.08 | 0.14 | 2.00 | 0.48 |
| 10 | 160 | 360 | d.w | 0 | 3.97 | 0.03 | 1.48 | 0.46 | 0.06 | 0.00 | 0.06 | 0.05 | 0.16 | 2.00 | 0.49 |
| 11 | 160 | 180 | 1 | 1.00 | 3.85 | 0.15 | 1.54 | 0.35 | 0.11 | 0.00 | 0.08 | 0.08 | 0.13 | 2.00 | 0.50 |
| 12 | 160 | 360 | d.w. | 0 | 3.94 | 0.06 | 1.46 | 0.45 | 0.08 | 0.00 | 0.03 | 0.14 | 0.10 | 2.00 | 0.51 |
| 13 | 160 | 90 | d.w. | 0 | 4.01 | 0.00 | 1.41 | 0.53 | 0.06 | 0.40 | 0.11 | 0.34 | 0.00 | 2.00 | 0.52 |
| 14 | 160 | 60 | d.w. | 0 | 3.81 | 0.19 | 1.55 | 0.35 | 0.11 | 0.00 | 0.07 | 0.07 | 0.17 | 2.00 | 0.53 |
| 15 | 160 | 180 | 1 | 1.00 | 3.87 | 0.13 | 1.28 | 0.41 | 0.32 | 0.00 | 0.12 | 0.08 | 0.13 | 2.00 | 0.54 |
| 16 | 80 | 90 | 0.01 | 1.00 | 3.91 | 0.09 | 1.48 | 0.45 | 0.07 | 0.00 | 0.06 | 0.08 | 0.16 | 2.00 | 0.54 |
| 17 | 160 | 90 | d.w. | 0 | 3.98 | 0.02 | 1.39 | 0.53 | 0.08 | 0.00 | 0.03 | 0.16 | 0.10 | 2.00 | 0.55 |
| 18 | 120 | 180 | 1 | 0.20 | 3.94 | 0.06 | 1.40 | 0.50 | 0.11 | 0.00 | 0.12 | 0.07 | 0.15 | 2.00 | 0.56 |
| 19 | 160 | 360 | d.w. | 0 | 3.89 | 0.11 | 1.46 | 0.46 | 0.08 | 0.00 | 0.04 | 0.17 | 0.10 | 2.00 | 0.56 |
| 20 | 120 | 90 | 100 | 0.01 | 3.92 | 0.08 | 1.31 | 0.49 | 0.20 | 0.00 | 0.06 | 0.09 | 0.16 | 2.00 | 0.56 |
| 21 | 160 | 90 | d.w. | 0 | 3.88 | 0.12 | 1.38 | 0.46 | 0.16 | 0.15 | 0.18 | 0.11 | 0.01 | 2.00 | 0.58 |
| 22 | 160 | 360 | 100 | 1.00 | 3.82 | 0.18 | 1.42 | 0.48 | 0.11 | 0.00 | 0.14 | 0.18 | 0.08 | 2.00 | 0.66 |
| 23 | 120 | 90 | 100 | 0.01 | 3.91 | 0.09 | 1.31 | 0.57 | 0.13 | 0.00 | 0.12 | 0.16 | 0.11 | 2.00 | 0.66 |
| 24 | 160 | 180 | 0.01 | 1.00 | 3.61 | 0.39 | 1.58 | 0.31 | 0.11 | 0.00 | 0.50 | 0.10 | 0.00 | 2.00 | 0.71 |
| 25 | 160 | 180 | 0.01 | 1.00 | 3.63 | 0.37 | 1.51 | 0.36 | 0.13 | 0.00 | 0.31 | 0.11 | 0.10 | 2.00 | 0.73 |
| 26 | 160 | 180 | 100 | 1.00 | 3.57 | 0.43 | 1.54 | 0.35 | 0.10 | 0.00 | 0.15 | 0.12 | 0.20 | 2.00 | 0.78 |
| 27 | 60 | 180 | 10 | 0.33 | 3.90 | 0.10 | 0.89 | 0.48 | 0.54 | 0.00 | 0.36 | 0.24 | 0.00 | 1.91 | 0.84 |

d.w. = deionized water.

produce electron diffraction patterns or the patterns deteriorate rapidly, indicating electron-beam damage. (4) Small flakes of <1 μm (Figure 7c) occur in products from temperatures of 120–160°C, reaction times of 180–360 d, and deionized water. Chemical compositions correspond to smectite-rich I-S and they have well-developed smectite-like electron diffraction patterns (*hk* rings). Note in Figure 7c that the particle is comprised of delicate laths.

## DISCUSSION

XRD detected a poorly crystalline phase with a peak at 10 Å in the starting material with the particle size range of 10–200 μm that corresponds to dehydroxylated smectite. This peak disappeared with increasing temperature and time, and in low-concentration solutions. As this peak diminished, a peak at 14 Å increased in intensity. The 14-Å peak moved to 17 Å upon glycolation, which is typical of smectite or smectite-rich I-S. Neither the peak at 10 Å nor that at 14 Å was detected for experiments with particle sizes of 20–60 μm. Thus, most of the newly formed I-S, although not all as indicated by electron microscopy, originated from the dehydroxylated smectite. I-S formed in experiments with the 20–60-μm size particles was below the detection limit of XRD probably because the dehydroxylated smectite was here in lower concentration.

The newly formed phase is random I-S with 75% smectite as determined by XRD (Figure 1) and AEM (Table 1). Some particles have a layer charge corresponding to either I-S with high proportions of illite or pure illite. Note that no particles were found with a smectite-like layer charge even at low temperature (60°C) or high Na/K ratios. Possibly, the smectite present in the tuff previous to calcination was in fact smectite-rich I-S, so that its dehydroxylate produced I-S during the experiments by rehydroxylation. Glycolated samples of the tuff showed that it was smectite or I-S with a maximum of 10% illite layers. Because the proportion of illite layers in the products is higher at 25%, it is concluded that the reaction conditions influenced the chemical composition of the products.

The particle-size distribution and particle-morphology analyses did not show appreciable differences between the starting materials and products, indicating that the alteration process was limited, in agreement with the XRD analysis, which detected very low (10–200 μm) or no (20–60 μm) I-S in the products. Glass dissolution and I-S formation did not occur sufficiently to change particle size or shape appreciably. However, some glass grains were fully altered to I-S with preservation of their original shape (*e.g.*, Figures 6f and 7b). If this is a common event, alteration may progress extensively without apparent changes in particle size and morphology.

The data suggest an alteration sequence in which I-S grows directly from the surface of glass grains. The hemispherical growths on grain surfaces are smectite-like in composition and are probably an intermediate stage of alteration (Figure 6b and 6c). Tazaki *et al.* (1989, 1992), in natural and experimentally altered volcanic glass, found hemispherical structures containing crystalline domains with 3.3–20-Å spacings. They interpreted these crystalline regions as clay precursors. Thus, the hemispherical structures that developed on the glass surface in our samples are probably zones where incipient clay formation is occurring. Fiore *et al.* (1999) observed large clay-mineral crystals forming within grains of rhyolitic obsidian altered at low temperature, which seems to be a further stage in this process of crystallization of clay minerals within glass particles. Direct formation of I-S on the surface of glass grains is also consistent with altered rims (Figure 7a) where there is a morphological and chemical evolution from glass at the core to I-S at the edges, and with particles consisting of I-S that preserve the original shape of the glass grains (Figures 6f and 7b).

There is also evidence that a second mechanism of glass dissolution and I-S precipitation operates. Very small flakes were observed on fresh grain surfaces (Figure 6d) that are interpreted to be I-S precipitated from solution. These flakes may be an early stage of alteration by surface transformation, but this is unlikely because the glass surfaces where these particles occur are fresh, without additional indications of alteration. These flakes were characterized in the SEM analysis and they could not be analyzed by EDS. Nevertheless, we assume these particles are I-S because all AEM analyses of similar flakes yielded an I-S composition. In summary, however, the direct transformation mechanism (*i.e.*, I-S crystallizing directly on glass-grain surfaces) operated more extensively than glass dissolution and I-S precipitation because the morphological features of the former process are more abundant.

## ACKNOWLEDGMENTS

We thank R. Klimentidis for reviewing the manuscript, V. Summa for assistance with the laser particle-size analysis, A. Vitoria for the preparation of thin sections, and A. Yebra for help with the computer program for image analysis. SEM-EDS studies were performed at the Dipartimento Geomineralogico (University of Bari, Italy). This work was financially supported by DGICYT, project PB94-0120.

## REFERENCES

Abdelouas, A., Crovisier, J., Lutze, W., Fritz, B., Mosser, A., and Müller, R. (1994) Formation of hydrotalcite-like compounds during R7T7 nuclear waste glass and basaltic glass alteration. *Clays and Clay Minerals,* **42,** 526–533.

Amouric, M. and Olives, J. (1991) Illitization of smectite as seen by high-resolution transmission electron microscopy. *European Journal of Mineralogy,* **3,** 831–835.

Banfield, J.F. and Barker, W.W. (1998) Low-temperature alteration in tuffs from Yucca Mountain, Nevada. *Clays and Clay Minerals,* **46,** 27–37.

Bellon, H. (1976) Séries magmatiques néogènes et quaternaires du pourtour de la Méditerranée occidentale, comparées dans leur cadre géochronométrique—implications géodinamiques. Ph.D. thesis, Université de Paris Sur, Paris, France, 367 pp.

Bellon, H., Bordet, P., and Montenat, C. (1983) Chronologie du magmatisme néogene des Cordillères Bétiques (Espagne meridionale). *Bulletin Societé Géologique de France,* **25,** 205–217.

Berkgaut, V., Singer, A., and Stahr, K. (1994) Palagonite reconsidered: Paracrystalline illite-smectites from regoliths on basic pyroclastics. *Clays and Clay Minerals,* **42,** 582–592.

Brindley, G.W. and Lemaitre, J. (1987) Thermal, oxidation and reduction reactions of clay minerals. In *Chemistry of Clays and Clay Minerals,* A.C.D. Newman, ed., Mineralogical Society, London, 319–370.

Caballero, E. (1985) Quimismo del proceso de bentonitización en la región volcánica de Cabo de Gata (Almería). Ph.D. thesis, Universidad de Granada, Granada, Spain, 338 pp.

Crovisier, J.L., Eberhart, J.P., Thomassin, J.H., Juteau, T., Touray, J.C., and Ehret, G. (1982) Interaction "eau de mer-verre basaltique" à 50°C. Formation d'un hydroxycarbonate et de produits silicatés amorphes (Al, Mg) et mal cristallisés (Al, Fe, Mg). Etude en microscopie électronique et par spectrométrie des photoélectrons (E.S.C.A.). *Comptes Rendus de l'Académie des Sciences de Paris, Série II,* **294,** 989–994.

Crovisier, J.L., Honnorez, J., and Fritz, B. (1992) Dissolution of subglacial volcanic glasses from Iceland: Laboratory study and modelling. *Applied Geochemistry,* Supplementary Issue, **1,** 55–81.

Di Battistini, G., Toscani, L., Iaccarino, S., and Villa, I.M. (1987) K/Ar ages and the geological setting of calc-alkaline volcanic rocks from Sierra de Gata, SE Spain. *Neues Jahrbuch für Mineralogie. Monatshefte,* **H8,** 337–383.

Drits, V.A., Salyn, A.L., and Šucha, V. (1996) Structural transformations of interstratified illite-smectites from Dolná Ves hydrothermal deposits: Dynamics and mechanisms. *Clays and Clay Minerals,* **44,** 181–190.

Farmer, V.C. (1974) The layer silicates. In *The Infrared Spectra of Minerals,* V.C. Farmer, ed., Mineralogical Society, London, 331–363.

Fernández Soler, J.M. (1992) El volcanismo calco-alcalino de Cabo de Gata (Almería). Ph.D. thesis, Universidad de Granada, Granada, Spain, 243 pp.

Fiore, S. (1993) The occurrences of smectite and illite in a pyroclastic deposit prior to weathering: Implications on the genesis of 2:1 clay minerals in volcanic soils. *Applied Clay Science,* **8,** 249–259.

Fiore, S., Huertas, F.J., Tazaki, K., Huertas, F., and Linares, J. (1999) A low temperature experimental alteration of a rhyolitic obsidian. *European Journal of Mineralogy,* **11,** 455–469.

Ghiara, M.R., Franco, E., Petti, C., Stanzione, D., and Valentino, G.M. (1993) Hydrothermal interaction between basaltic glass, deionized water and seawater. *Chemical Geology,* **104,** 125–138.

Hall, A. (1998) Zeolitization of volcaniclastic sediments: The role of temperature and pH. *Journal of Sedimentary Research,* **68,** 739–745.

Hofmann, F. and Jager, E. (1959) Saponite as an alteration product of basaltic tuff at Karolihof. *Schweizerische Mineralogische und Petrographische Mitteilungen,* **39,** 117–124.

Inoue, A., Watanabe, T., Kohoyama, N., and Brusewitz, A.M. (1990) Characterization of illitization of smectite in bentonite beds at Kinnekulle, Sweden. *Clays and Clay Minerals,* **38,** 241–249.

Inoue, A., Utada, M., and Wakita, K. (1992) Smectite-to-illite conversion in natural hydrothermal systems. *Applied Clay Science,* **7,** 131–145.

Kawano, M. and Tomita, K. (1992) Formation of allophane and beidellite during hydrothermal alteration of volcanic glass below 200°C. *Clays and Clay Minerals,* **40,** 666–674.

Kawano, M. and Tomita, K. (1995) Experimental study on the formation of clay minerals from obsidian by interaction with acid solution at 150° and 200°C. *Clays and Clay Minerals,* **41,** 212–222.

Kawano, M. and Tomita, K. (1997) Experimental study of the formation of zeolites from obsidian by interaction with NaOH and KOH solutions at 150 and 200°C. *Clays and Clay Minerals,* **45,** 365–377.

Kawano, M., Tomita, K., and Kamino, Y. (1993) Formation of clay minerals during low temperature. Experimental alteration of obsidian. *Clays and Clay Minerals,* **41,** 431–441.

Kawano, M., Tomita, K., and Shinohara, Y. (1997) Analytical electron microscopic study of the noncrystalline products formed at early weathering stages of volcanic glass. *Clays and Clay Minerals,* **45,** 440–447.

Keene, J.B., Clague, D.A., and Nishimori, R.K. (1976) Experimental hydrothermal alteration of tholeiitic basalt: Resultant mineralogy and textures. *Journal of Sedimentary Petrology,* **46,** 647–653.

Lanson, B. and Champion, D. (1991) The I/S-to-illite reaction in the late stage diagenesis. *American Journal of Science,* **291,** 473–506.

Linares, J. (1985) The process of bentonite formation in Cabo de Gata, Almería, Spain. *Mineralogica et Petrographica Acta,* **29-A,** 17–33.

Mackenzie, R.C. (1970) Simple phyllosilicates based on gibbsite- and brucite-like sheets. In *Differential Thermal Analysis, Volume 1. Fundamental Aspects,* R.C. Mackenzie, ed., Academic Press, London, 504–514.

Magonthier, M.C., Petit, J.C., and Dran, J.C. (1992) Rhyolitic glasses as natural analogues of nuclear waste glasses: Behaviour of an Icelandic glass upon natural aqueous corrosion. *Applied Geochemistry,* Supplementary Issue, **1,** 83–93.

Mariner, R.H. and Surdam, R.C. (1970) Alkalinity and formation of zeolites in saline alkaline lakes. *Science,* **170,** 977–980.

McDaniel, P.A., Falen, A.L., Tice, K.R., Graham, R.C., and Fendorf, S.E. (1995) Beidellite in E horizons of northern Idaho spodosols formed in volcanic ash. *Clays and Clay Minerals,* **43,** 525–532.

Nagasawa, K. (1978) Kaolin Minerals. In *Clays and Clay Minerals of Japan. Developments in Sedimentology, Volume 26,* T. Sudo and S. Shimoda, eds., Elsevier, New York, 189–219.

Shapiro, L. (1975) *Rapid Analysis of Silicate, Carbonate, and Phosphate Rocks.* U.S. Geological Survey Bulletin 1401, Washington D.C., 76 pp.

Šucha, V., Kraus, I., Gerthofferová, H., Peteš, J., and Serekoová, M. (1993) Smectite to illite conversion in bentonites and shales of the east Slovak Basin. *Clay Minerals,* **28,** 243–253.

Tazaki, K., Fyfe, W.S., and van der Gaast, S.J. (1989) Growth of clay minerals in natural and synthetic glasses. *Clays and Clay Minerals,* **37,** 348–354.

Tazaki, K., Tiba, T., Aratani, M., and Miyachi, M. (1992) Structural water in volcanic glass. *Clays and Clay Minerals,* **40,** 122–127.

Thomassin, J.H., Boutonnat, F., Touray, J.C., and Baillif, P. (1989) Geochemical role of the water/rock ratio during the experimental alteration of a synthetic basaltic glass at 50°C. An XPS and STEM investigation. *European Journal of Mineralogy,* **1,** 261–274.

Tomita, K., Yamane, H., and Kawano, M. (1993) Synthesis of smectite from volcanic glass at low temperature. *Clays and Clay Minerals,* **41,** 655–661.

Wada, K. (1987) Minerals formed and mineral formation from volcanic ash by weathering. *Chemical Geology,* **60,** 17–28.

Zevenbergen, C., Van Reeuwijk, L.P., Bradley, J.P., Bloemen, P., and Comans, R.N.J. (1996) Mechanism and conditions of clay formation during natural weathering of MSWI bottom ash. *Clays and Clay Minerals,* **44,** 546–552.

E-mail of corresponding author: sandra@eez.csic.es

*(Received 8 July 1999; accepted 25 January 2000; Ms. 360; A.E. Stephen Altaner)*